Article

Electrical Resistivity Tomography and Induced Polarization for Mapping the Subsurface of Alluvial Fans: A Case Study in Punata (Bolivia)

Andres Gonzales Amaya [1,2,*], Torleif Dahlin [1], Gerhard Barmen [1] and Jan-Erik Rosberg [1]

[1]   Teknisk Geologi, Lund University, Box 118, Lund SE-22100, Sweden; torleif.dahlin@tg.lth.se (T.D.);
      gerhard.barmen@tg.lth.se (G.B.); jan-erik.rosberg@tg.lth.se (J.-E.R.)
[2]   Laboratorio de Hidraulica, Universidad Mayor de San Simon,
      Av. Petrolera km 4.2, 6760 Cochabamba, Bolivia
*   Correspondence: andres.gonzales@tg.lth.se; Tel.: +46-222-7425

Abstract: Conceptual models of aquifer systems can be refined and complemented with geophysical data, and they can assist in understanding hydrogeological properties such as groundwater storage capacity. This research attempts to use geoelectrical methods, Electrical Resistivity Tomography and Induced Polarization parameters, for mapping the subsurface in alluvial fans and to demonstrate its applicability; the Punata alluvial fan was used as a case study. The resistivity measurements proved to be a good tool for mapping the subsurface in the fan, especially when used in combination with Induced Polarization parameters (i.e., Normalized Chargeability). The Punata alluvial fan characterization indicated that the top part of the subsurface is composed of boulders in a matrix of finer particles and that the grain size decreases with depth; the electrical resistivity of these deposits ranged from 200 to 1000 Ωm, while the values of normalized chargeability were lower than 0.05 mS/m. The bottom of the aquifer system consisted of a layer with high clay content, and the resistivity ranged from 10 to 100 Ωm, while the normalized chargeability is higher than 0.07 mS/m. With the integration of these results and lithological information, a refined conceptual model is proposed; this model gives a more detailed description of the local aquifer system. It can be concluded that geoelectrical methods are useful for mapping aquifer systems in alluvial fans.

Keywords: alluvial fan; electrical resistivity tomography; induced polarization

1. Introduction

Alluvial fans are sedimentary deposits of boulders, gravel, sand, and finer sediments. They are formed at the foot of mountains, as a river emerges from the mountain range and flows into a large valley, water body, or an area where the river slope decreases [1–4]. The genesis of alluvial fans creates deposits with different permeability and porosity due to ancient streams and mud flow events. The permeability of these deposits depends on effective porosity and the interstitial pore space size: stream flow deposits have larger spaces between grains, while mudflow deposits have smaller interstitial openings. Therefore, stream flow deposits are good aquifers, while mudflow deposits are ideal aquicludes [2,5].

The mapping of the aquifer geometry (layering, thickness, and boundary conditions) in alluvial fans is a key process for estimating important physical properties, such as storage volume, groundwater flow patterns, and recharge/discharge process. This information is important from a hydrogeological point of view, since available water reserves can be estimated. Information from the local geology, drilling reports, and pumping tests are the most common methods for determining these physical

properties. However, these techniques are time demanding and provide punctual data, therefore they could be used in combination with geophysical methods to save time and generate continuous data along a profile [6,7].

Geoelectrical methods are near surface geophysical techniques for engineering and environmental applications [8,9]. In the last few decades the development of multi-electrode arrays, automatized acquisition systems, and new inversion algorithms have renewed the interest in these methods. Electrical Resistivity Tomography (ERT) is one of the most commonly used geophysical methods for imaging subsurface features. This technique estimates the distribution in resistivity of the ground, which can vary with water content and lithology. The resistivity distribution can be interpreted from a hydrogeological point of view [10]. In the ERT surveys, the measured quantity is called apparent resistivity ("ρ_a"), which is the equivalent resistivity for a homogeneous soil volume which yields the same potential value as the true model. In order to estimate the true resistivity distribution, an inverse numerical modeling (inversion) is used to create a model based on the apparent resistivity data [11]. The inversion adjusts a finite difference or finite element model in an iterative process [11–14] by comparing the measured apparent resistivity versus the calculated resistivity from the inverted model. The use of ERT profiles and additional data from the subsurface, such as drilling reports and borehole loggings, makes it possible to estimate the thickness, depth, and morphology of different units of the subsurface [6,7,15].

The Induced Polarization (IP) effect is a measure of the soil ability to be polarized when it is under the influence of an electric field; in other words, it means that during the polarization the energy is stored reversibly in the soil [16]. For this research, the measurements of IP have been carried out in the time domain. The Time-Domain IP (TDIP) surveys are carried out by transmitting current into the ground while potential difference is measured to determinate the resistivity. After the current is turned off, the potential decay in the ground is measured again in one or several intervals of time windows. A common parameter used to quantify TDIP measurements is the chargeability, which is defined as the ratio of the secondary potential over the primary potential of the transmitted current. For measuring the secondary potential, a discrete integration is often used with potential readings recorded in logarithmically spaced time gates. The gating, and the duration of the current pulses and off-times have an important effect on the magnitude of the integral chargeability [17–19]. Therefore, it is often ambiguous to compare chargeability values between different surveys; while resistivity is a material parameter, integral chargeability is highly dependent on measurement settings.

Dividing the chargeability with the measured resistivity yields the normalized chargeability, which might highlight areas with high surface conductance properties [17,20]. This assumption is valid for soil free of metal, where electronic conduction in solid material is negligible. IP surveys have proved to be a useful tool for mapping lithological layers of unconsolidated sediments; moreover, it provides an important parameter which can be used to resolve ambiguities in the interpretation of the results from other geophysical methods [21].

Interpretation of IP parameters in geological materials might be complicated due to the heterogeneity of soils and rocks at the micro-scale, where polarization process occurs. Furthermore, mineral composition, micro-geometry, chemical environmental, and other parameters make it difficult to understand exactly how the polarization mechanism works. A lot of efforts have been dedicated in the last few years to get a better understanding of this, ending in groundbreaking results such as the relationships between electrical measurements and petrophysical parameters found by many authors [22–24]. High normalized chargeability values have been observed for sediments with high clay content, while soils with uniform particle size of sand and gravel commonly yield lower normalized chargeability values [21]. This contrast of normalized chargeability values could be used to interpret geological units and determine potential aquifers.

The Punata alluvial fan is an agricultural region and it is characterized by a semi-arid climate with low average annual precipitation (around 350 mm/year) [25,26]. The rapid agricultural development in the area has caused a high increase in demand for water supply. Therefore, the drilling of wells has

increased considerably in recent years—by the year 2015 the estimated number of wells was around 355 [25]. The monitoring of the groundwater level shows a decreasing trend of the water table, and probably the main reason for this decline is due to the fact that groundwater extraction has equaled or exceeded the natural recharge during the last few years. Worldwide, many geoelectrical surveys have been applied in a wide range of geological studies [6,8,17,27], but there has not been any research that has used ERT and IP in Bolivia, according to our knowledge. In the Punata alluvial fan (Figure 1), despite several boreholes with drilling report and well resistivity logging being available, the real geometry of the aquifer system is partially unknown. In order to fill in the gaps and demonstrate the applicability of indirect data retrieved from geoelectrical methods in alluvial fans, a case study was carried out in this area.
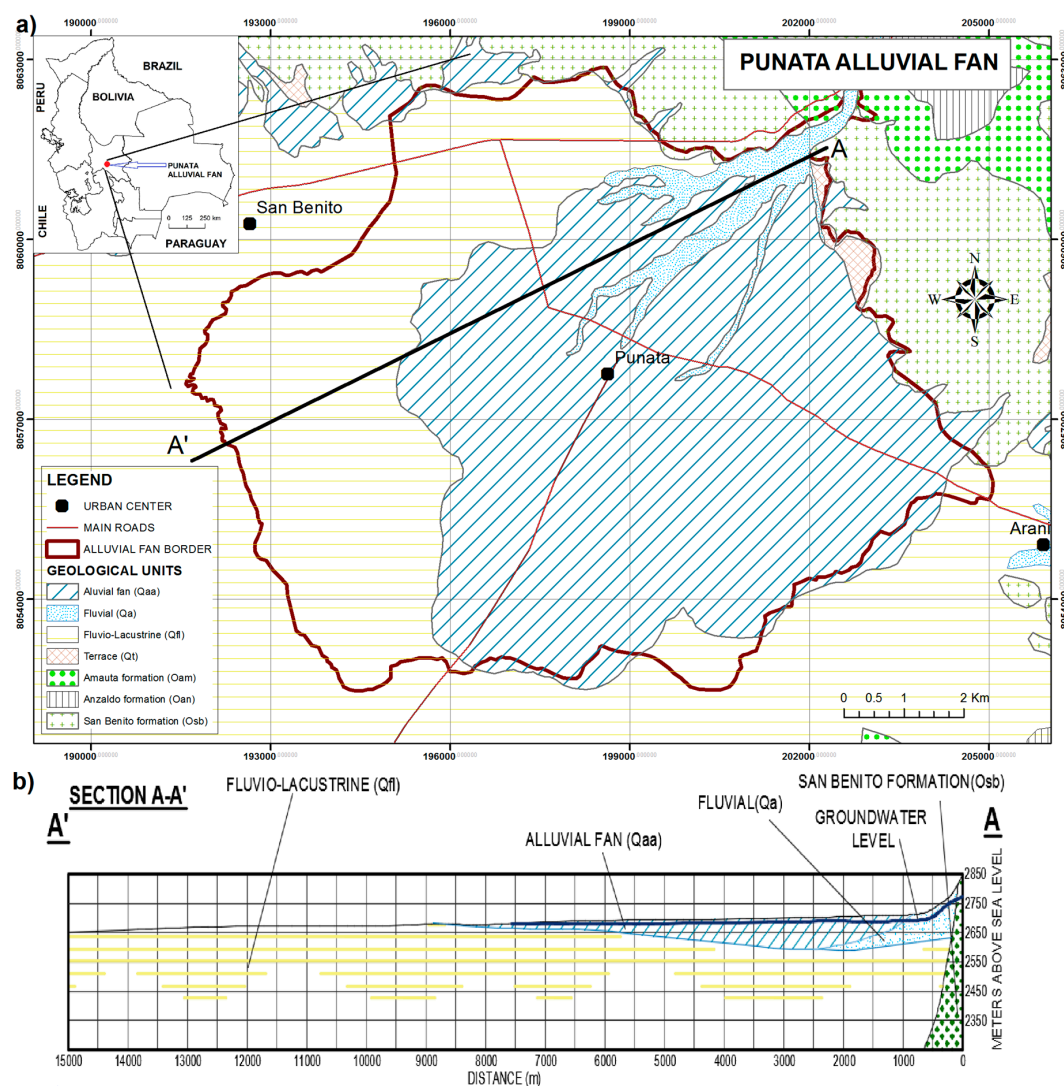

Figure 1. (**a**) Location of the study area in the central part of Bolivia and regional geology overview, modified from SERGEOMIN [28]; (**b**) Cross section of the study area, from UNDP-GEOBOL [26].

The first objective of this paper is to demonstrate the applicability of the ERT technique for mapping aquifer systems located in alluvial fans, in terms of layering and layer thickness. The second objective is to test if normalized chargeability results can be used for solving ambiguities during the ERT interpretation process in alluvial fan environments. The last objective of this research is to propose a refined conceptual model of the study area by integrating the ground truth data and the interpretation of resistivity and induced polarization parameters; the proposed conceptual model

will help in contributing and improving upon the knowledge regarding the extension of the different geological units.

2. Study Area and Geological Settings

The Punata alluvial fan is located in the central part of Bolivia (Figure 1a), in the department of Cochabamba. The alluvial fan is flanked in the north and east by the Tunari mountainous massif, whose peaks can reach 3500 meters above sea level (m a.s.l.). From the southeast to the west, the fan is limited by a clay fringe. The topography is gently sloping from the northeast to southwest, with altitudes around 2700 m a.s.l. The extension of the alluvial fan is around 90 km^2. The main urban center is Punata city in the middle of the fan. The groundwater level varies from 35–40 to 10–15 m below surface in the apex and middle/distal part of the fan, respectively (Figure 1b).

The regional geology is described by UNDP-GEOBOL [26]. The mountainous massif is formed by Ordovician rocks—Anzaldo (Oan), Amauta (Oam), and San Benito (Osb) formations—while the valleys are filled with unconsolidated sediments (Quaternary deposits). During the lower Pliocene, due to the lifting of the mountain massif, tectonic valleys and enclosed lakes were created. The weather in this period was predominately dry, therefore saline material with high clay content was deposited [26,29,30]. The report of UNDP-GEOBOL [26] found water conductivity values for borehole P305 of 9.7 mS/m between 0 to 100 m depth, 600 mS/m at 150 m depth and 3000 mS/m at 250 m depth, which indicates an increase of salinization with depth.

The depth to the bedrock within the fan is not yet defined, but some reports [26,28] estimate that the thickness of the sediments may be greater than 300 m. The description of the geological units in the alluvial fan are:

- Alluvial fan deposits (Qaa): Coarse grained materials, composed of boulders, gravel, and sand, forming alluvial fans and river channel deposits. Silt and clay are deposited in the top parts.
- Fluvial deposits (Qa): Boulders, gravel, and sand are the main materials which were transported and deposited by streams.
- Fluvio-lacustrine deposits (Qfl): Fine materials, consisting of clay and fine sand with intercalation of organic horizons and dark blue clays.
- Terrace deposits (Qt): Angular boulders of variable size, mixed with silt and sandy materials. These deposits cover the zones in the northeastern edge of the alluvial fan.

3. Methods

3.1. Data Acquisition

A total of 30 ERT surveys were measured in the Punata alluvial fan (Figure 2). All data were measured using an ABEM Terrameter LS equipment. Stainless steel electrodes and four electrode cables with 21 take-outs each were used. The maximum separation between electrodes was 10 s, providing a total spread length of 800 s between the outermost electrodes. A total of 49,403 data points were collected, the length of each survey is listed in Table 1. During the ERT surveys, the Multiple Gradient array was used; this array has proved to be more suitable for multichannel data acquisition providing a significant increase in the velocity of data acquisition and giving a higher density of data points [31,32]. Elevations and coordinates of the electrodes were collected with a GPS and a Digital Elevation Model with a spatial resolution of 30 m × 30 m; the topography was included in the files before the inversion [33].

The current and voltage transmitted in each survey depended on the ground conditions (electrode to ground contact resistance) and they varied from 5 to 200 mA and from 10 to 300 V, respectively. In some surveys, when time allowed, data acquisition was done with combined measurement of resistivity and chargeability (refer to Table 1). The timing setup used for these surveys applied a current-on of 1 s (with an acquisition delay time of 0.4 s and an acquisition time of 0.6 s) and a current-off of 1 s. A total of nine time windows were measured, where each window time is a multiple

period time of 20 ms in order to suppress any power line noise [34]. The selection of the ERT locations was predominately planned according to the availability of areas free of obstacles such as houses, fences, crops, and paved roads; another problem confronted was getting the permission of land owners to perform the surveys in their lands. When conditions allowed, the roll-along technique was applied for getting continuous profiles.
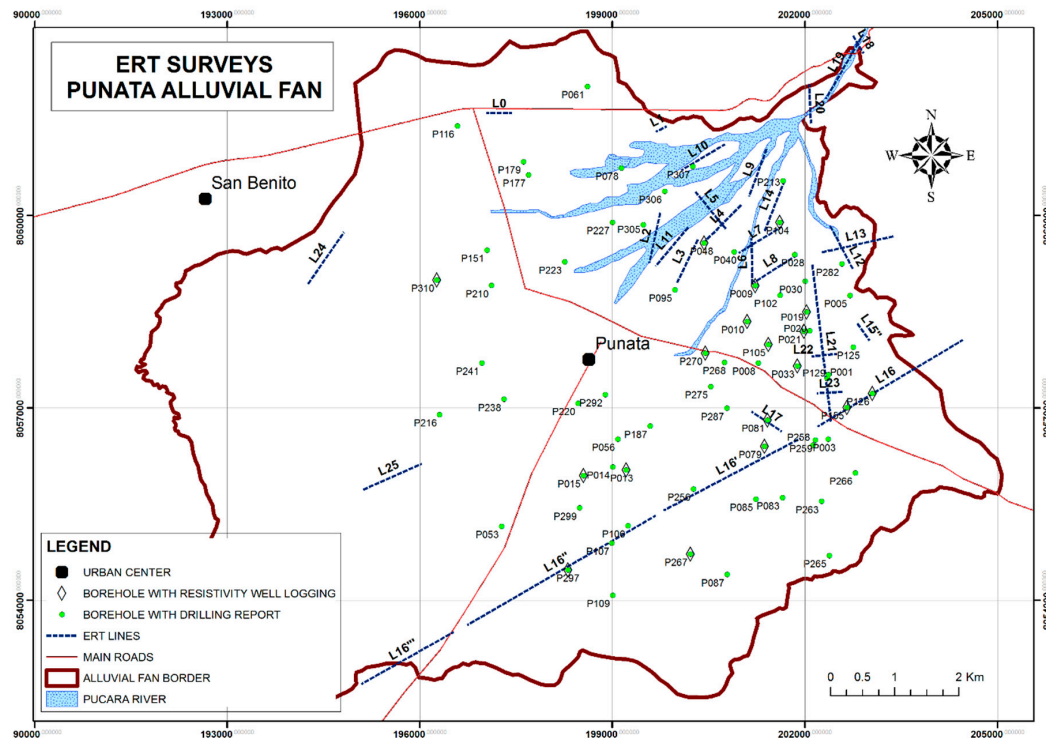

Figure 2. Electrical Resistivity Tomography (ERT) surveys performed in the Punata alluvial fan. The green dots stand for boreholes with drilling reports and the diamonds represent geophysical well-loggings.

3.2. Data Processing and Inversion

The collected field data were quality checked using visual tools such as pseudosection plots and multi profile plots. The measured apparent chargeability time window data were averaged to integral chargeability. Data were inverted using RES2DINV, version 4.02.02; this program supports several types of arrays, and has been optimized for the inversion of large data sets [35]. The Robust Inversion (L1-norm) option was used as it is less sensitive to noisy data [11,14]. For the model discretization, a setup of the model refinement with cell widths of half the unit spacing was used. For the damping parameter option, a vertical/horizontal flatness ratio of 0.25 was used, since the subsoil layers in the Punata alluvial fan tend to be predominantly horizontal, hence low values for this filter are advised.

In addition to ERT surveys, data from drilling reports and geophysical well loggings were used in order to validate and interpret ERT results. This was done for ERT sections sufficiently close to (or at) the same location as the borehole logging points.

4. Results

After the data inversion, surveys with high root mean square (RMS) errors where omitted; the source of these errors might be due to bad contact between the electrodes and the ground. The number of iterations for each survey was seven; all the displayed surveys present RMS errors lower than 10.0% (Table 1). The calculated resistivity from ERT surveys predominately ranged from 50 to 1000 Ωm.

Table 1. ERT surveys with RMS error lower than 10%. Where Res. stands for resistivity and I.P. for induced polarization.

Profile	Length (m)	Data Points	RMS Error (%)		Profile	Length (m)	Data Points	RMS Error (%)	
			Res.	I.P.				Res.	I.P.
L0	400	420	1.5	0.4	L16'	2600	7215	2.0	2.4
L2	800	509	3.0	-	L16''	3200	8812	6.9	-
L4	800	1030	1.5	0.6	L16'''	1400	3272	5.2	-
L5	800	952	3.5	-	L17	600	1030	1.1	-
L6	800	1030	5.3	6.0	L18	200	457	2.7	-
L7	800	752	3.4	-	L19	1000	2073	2.1	-
L8	800	1030	3.2	1.5	L20	400	1120	5.8	-
L12	800	1030	3.6	-	L21	2200	6083	1.5	2.8
L14	800	1030	1.8	-	L22	400	512	1.3	7.1
L15''	100	431	4.7	-	L23	400	512	1.5	2.3
L15'''	400	512	1.2	-	L24	1000	1898	7.8	-
L16	2400	6013	9.6	-	L25	1000	1680	9.1	7.4

A few soil samples were taken and the results are summarized in Table 2. Percentages of gravel, sand, silt, and clay were obtained; the porosity, bulk, and particle density were obtained as well. Soils B and C were mainly composed of fine sediments, while soils A and D were composed of coarse materials. The texture of these soil can be visualized in Figure 3.

Table 2. Grain size distribution and physical properties of soils in the surroundings of Line 15.

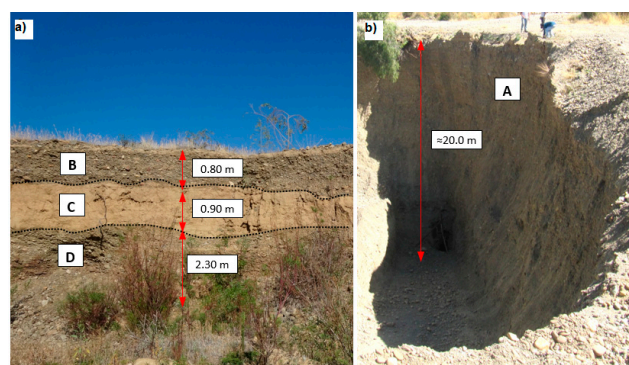| Soil	Gravel (%)	Sand (%)	Silt (%)	Clay (%)	Bulk Density (g/cm^3)	Particle Density (g/cm^3)	Total Porosity (%)
A	90.1	1.2	1.2	7.5	1.6	2.7	38.1
B	5.4	25.5	40.7	28.4	1.4	2.7	26.0
C	0.0	26.0	53.0	21.0	1.4	2.6	25.4
D	69.6	4.6	5.4	20.4	1.6	2.6	37.2

Figure 3. Typical stratigraphy in the Punata alluvial fan. (**a**) The soil profile displays a layer with three different soils (B, C, and D); while (**b**) shows a pit with a soil type A (coarse soil, composed by boulders and gravels).

On Figure 4, the results of three ERT surveys are shown; these profiles are selected because drilling and logging reports are available from the wells located close to the profile line, which helps in the understanding and interpretation process. The calculated resistivity is displayed on the left and the normalized chargeability on the right. At first sight, there is a clear trend of high resistivity values at the top in the different sections (values from 200 up to 1000 Ωm), while at the bottom, the resistivity values tend to decrease (values lower than 100 Ωm). Conversely, low values of normalized chargeability were found on the top layers, while higher values are in the bottom layers.
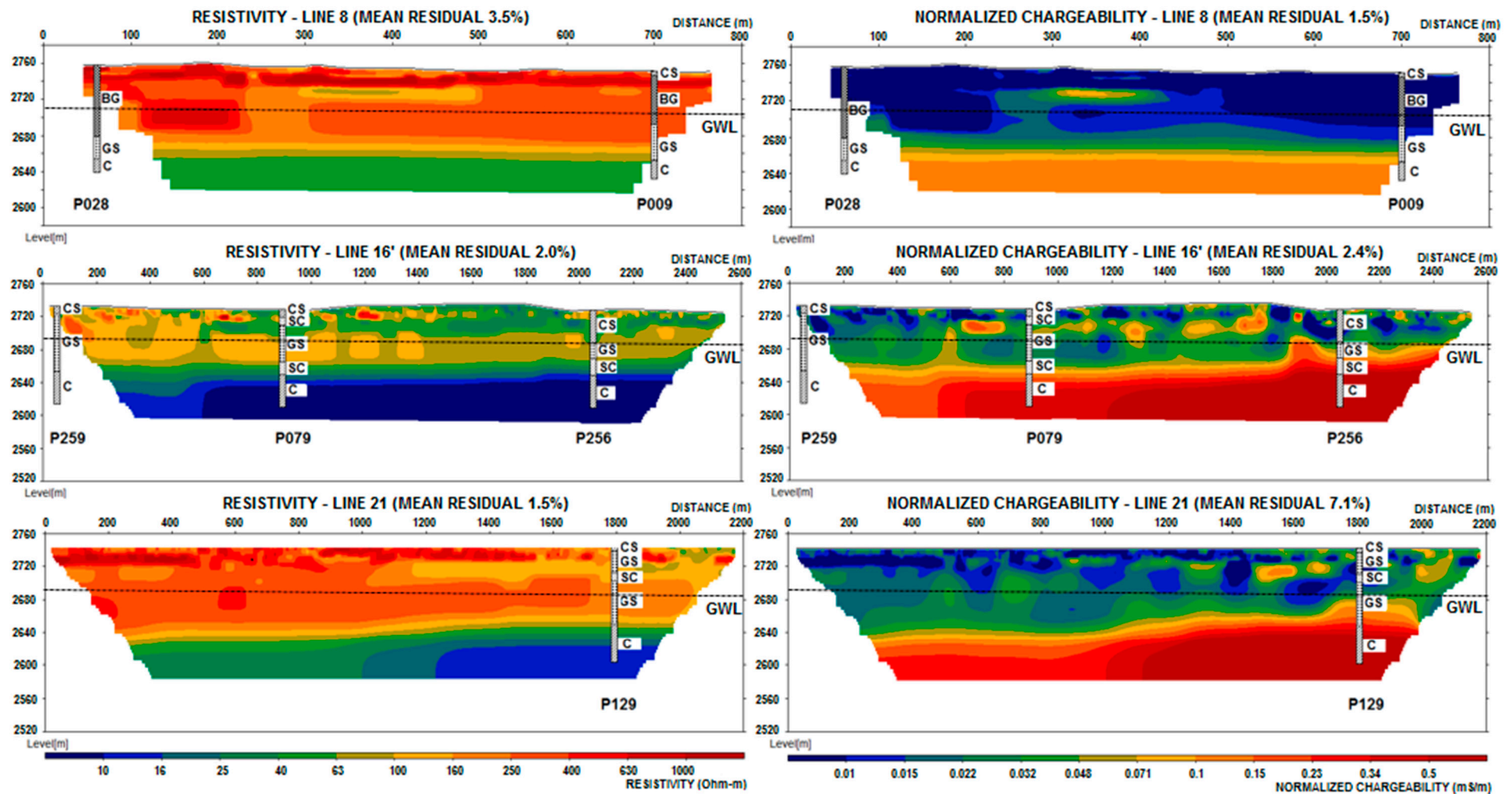
Figure 4. ERT surveys with a multiple gradient array protocol for Lines 8, 16', and 21; graphs on the left show inverted ERT and graphs on the right show normalized chargeability. The lithological description of available boreholes close to the surveys and the groundwater level (GWL) are included. Note different scales in axis *X* and *Y*.

Lithological information from wells located close to the lines are included in the figures, and the main material of each layer is shown by their initial letter (i.e., B stands for boulders, G for gravel, S for sand, and C for clay); for instance, a layer with the letters BG means that the material in that layer is mainly composed of boulders and gravel. The lithology describes a gradation of grains from coarse at the top, to fine grains at the bottom. The groundwater level is also included in the profiles.

In order to improve the interpretation of the ERT profiles, resistivity loggings were used to obtain a better description of the subsurface layering. In Figure 5, resistivity from the well loggings and from the ERT surveys are plotted; in addition, the normalized chargeability model is plotted. The lithology for each site is also included. There is, of course, some difference in the degree of detail between resistivity curves extracted from the ERT and the borehole measurements, but both curves follow the same trend. In both plotted curves, the resistivity decreases when it reaches the deepest levels. At the shallow levels the resistivity is high which is a possible indicator of coarse materials such boulder and gravel, which indicates a relatively high porostiy [36].
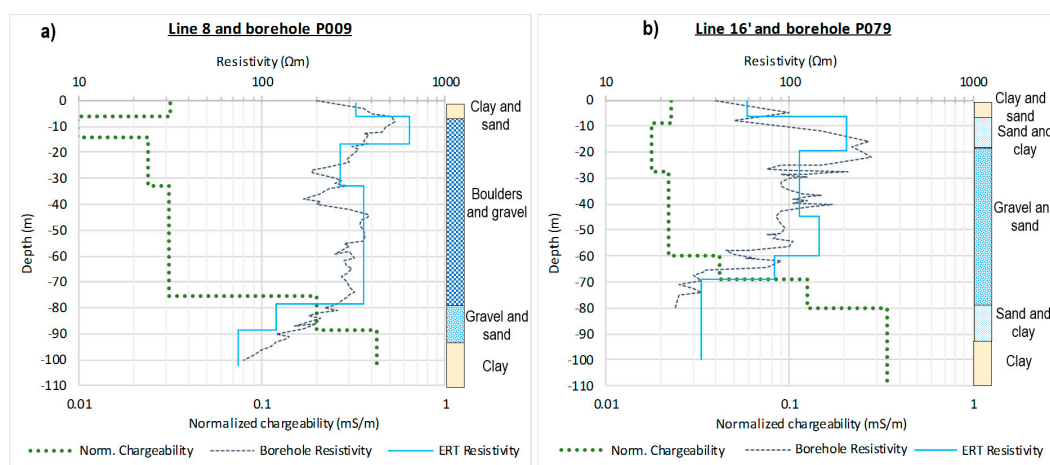

Figure 5. ERT resistivity is plotted versus the normalized chargeability and the resistivity from well-logging at the same position. (**a**) Line 8 and borehole P009; (**b**) Line 16′ and borehole P079.

5. Interpretation and Discussion

Characterization of the subsoil by resistivity methods in the Andean region were performed by many authors [37–39], where the results yield typical values of high resistivity when gravel and sand are the main content; when clay is the main compound low resistivity were obtained. In the Punata alluvial fan, the resistivity results were analyzed and the same tendency was observed. Assuming that the clay mineralogy is similar within the area, a correlation of low resistivity with high clay content can be assumed. However, if this assumption is accepted without making further analysis within the study area, the interpretation might be partially or completely wrong. Therefore, additional data such as lithological information from wells and other geophysical methods must be integrated for improving the interpretation of resistivity results. In Figures 4 and 5 the lithological information is added; it helps in understanding that high resistivity results are obtained in the top layers, and that these layers are most likely to have boulders and gravel. On the contrary, low values of resistivity were found where clay content is higher. The presence of clay deposits at the bottom of the lithology logs might be explained by the deposition of fine material from paleolakes in the Pliocene [26,28,29]. The high clay content and groundwater salinization might lead to low resistivity at the bottom of the ERT sections [40,41]. Flash floods on alluvial fans tend to deposit coarse material, leading to high resistivity at the top of ERT sections [36]. The clay content determined by UNDP-GEOBOL [26] in the top layers is less than 15%, and might be caused by flash floods, while in the bottom layers the clay content is greater than 40% and increases downwards, caused by a dry lacustrine environment.

Parkhomenko [42] noticed that chargeability values increased with clay content and water content, and that salinity and composition of the electrolyte have a direct influence on the occurrence of maximum chargeability values. In the present study, the chargeability results did not contribute to the interpretation of the geological features. However, when the normalized chargeability results were analyzed it was found that there was a clear difference of normalized chargeability values in layers with high clay content and coarse material; normalized chargeability can be highly dependent on clay minerology and clay content (e.g., [22,23,43]). The results of normalized chargeability (Figures 4 and 5) show a clear trend of increasing values in layers with high clay content, and lower values when coarse material is the main soil content. Keller and Frischknecht [44] found that the grain size of soils affects the normalized chargeability; in other words, the normalized chargeability shows low values when uniform particle sizes of sand and gravel are present, whereas for fine grains the values are greater. Slater and Lesmes [20] highlighted that the normalized chargeability parameter is independent of the bulk conduction effects and more sensitive to the surface chemical properties of the material. They performed an experiment where they did not find a clear correlation between resistivity and clay content, but obtained a good correlation between the normalized chargeability and clay content. Figure 5 shows the same trend in that when coarse material is the main compound of the soil at the top layers, high resistivity and low normalized chargeability values were obtained. While in the bottom layer, where clay was the main soil compound, the values of resistivity were low and the normalized chargeability values were high, and this is because clay particles have higher conductance surface and minerals which help in the particle charging process.

The interpretation of ERT results was made together with the normalized chargeability; Figures 6a and 7a show how ERT profiles have been interpreted and classified. According to the lithological reports, the bottom of the profiles was formed by lacustrine deposits (high clay content) and yields resistivity values lower than 40 Ωm (green and blue zones). The top layers were mainly composed of fluvial deposits (boulders and gravel), and the resistivity values were higher than 100 Ωm (yellow and red zones). Resistivity values between 40 to 100 Ωm might be associated with alluvial fan deposits (mix of clay and sand). The clay content increased towards southwest direction and with depth (refer to the sketch at the bottom right of Figure 6). Figure 6b demonstrates how the normalized chargeability can assist during the interpretation process in clarifying the differences between the areas with high clay content (high values at the bottom of profile) and coarse material (low values at the top of profile).
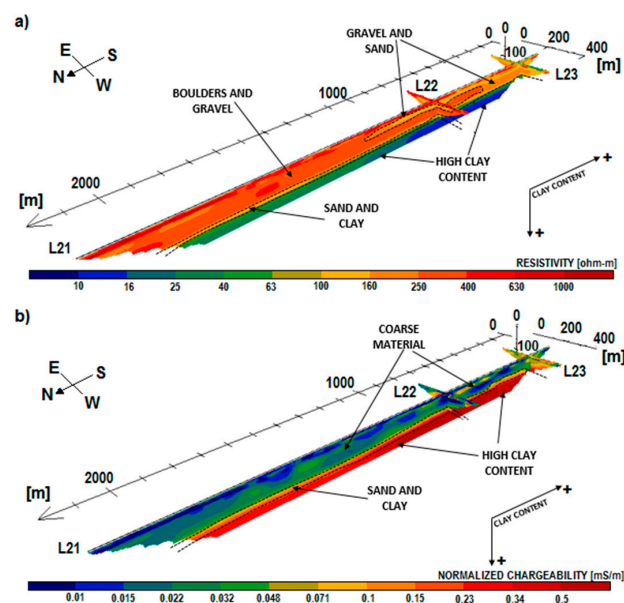

Figure 6. (**a**) Interpretation and 3D visualization of ERT profiles; (**b**) Interpretation and 3D visualization of normalized chargeability profiles. In both cases the lines are 21, 22, and 23.

　　　The interpretation of the results from the geoelectric surveys has contributed to the mapping of the aquifer system within the study area. The top layer might be considered to be a potential aquifer for groundwater extraction because it is composed of coarse grained material with high porosity. The thickness of this top layer decreases towards the distal part of the fan. On average the thickness varies from 40 to 120 s. The bottom layer with high clay content can be considered to be the bottom confining unit of the aquifer system. The thickness of this layer increases towards the distal part of the fan and becomes shallower—this can be visualized in Figure 7a (bluish bottom layer) and Figure 7b (yellow dashed pattern).

　　　From this information it is possible to refine and extend the actual conceptual model given by UNDP-GEOBOL [26]. Figure 7b shows the interpretation of the hydrological units derived from the integration of ERT (Figure 7a), normalized chargeability, and borehole information; these sections are located longitudinally in the fan (Line 16, 16′, 16″, and 16‴). This refined model shows that the top part of the aquifer system is composed mainly of coarse material, such as boulders and gravel, with a thickness between 40 to 120 m. In the fan head, this layer is an unconfined unit, and towards the distal part it becomes confined by a clay layer. Lenses of sand and clay might be found in this layer, however, the thickness of these lenses compared to the thickness of the coarse layer makes them negligible for the scope of this research, which is to map the aquifer system. Below the coarse layer, the soil grains reduce in size and it becomes more likely to find sand in a matrix of finer sediments. In the bottom of the system, the material has a high clay and silt content, with thickness greater than 200 m [26].
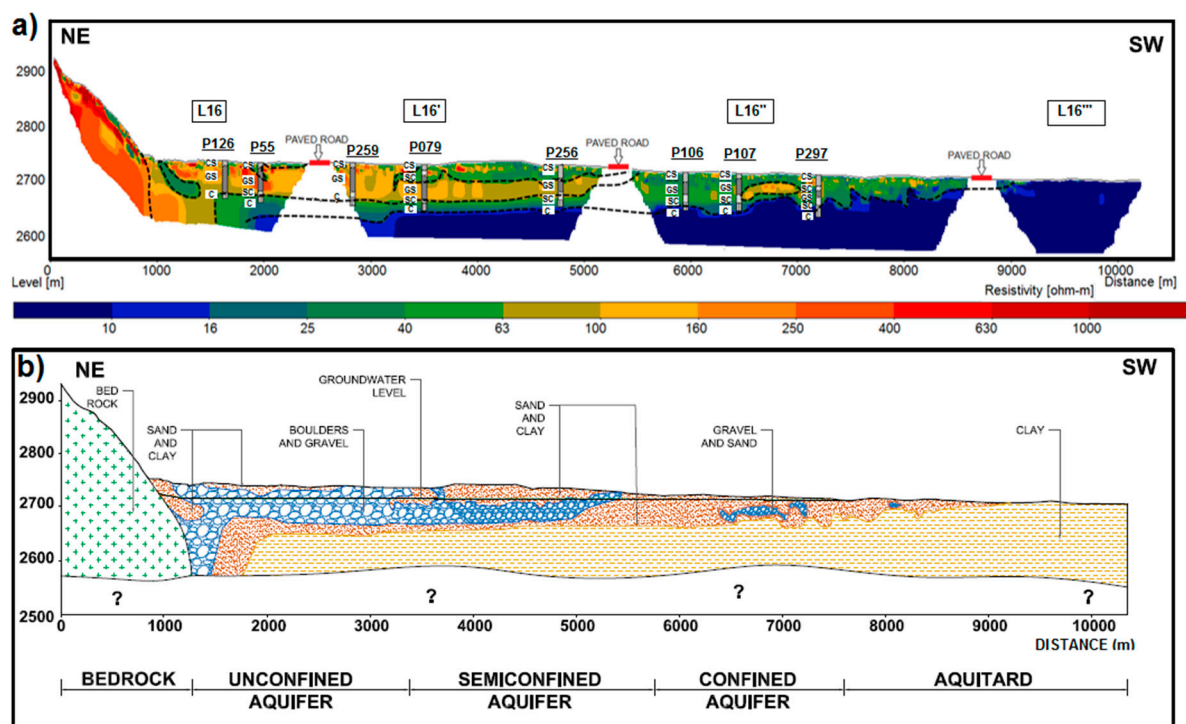

Figure 7. (**a**) Calculated resistivity along the line L16; the dashed lines are the proposed limits for the different units. (**b**) Proposed conceptual model and aquifer system in the Punata alluvial fan. The aquifer units are composed of boulders, gravel, and sand (blue pattern in Figure 7b).

　　　The refined conceptual model (Figure 7b) has a more reliable thickness for the different geological units. Moreover, a layer of sand in a matrix of finer sediments was distinguished just above the layer with high clay content. In addition, it was noticed that the thickness of the coarse layer becomes thinner towards the distal part, while the high clay content layer forming the bottom of the aquifer becomes shallower.

6. Conclusions

The geometry of the aquifer system in the Punata alluvial fan is partly unknown, hence ERT surveys were performed and proved to be a suitable tool for imaging the subsurface of alluvial fans. High resistivity values were generally obtained in the top layers, and values decreased with depth. In addition, geophysical well loggings were analyzed, and the same trend with resistivity values decreasing with depth was found. The normalized chargeability showed consistent response when layers with clay content were reached. Normalized chargeability, which is a measure of surface polarization processes, was useful during the ERT interpretation for solving ambiguities. All the surveys obtained high values of normalized chargeability at the bottom of the profiles; this is most likely due to the large and chargeable surface of the clay particles and the clay mineral composition. The integration of lithology, well loggings, and geoelectrical measurements yielded useful information for refining the hydrogeological model of the Punata alluvial fan. In general, in the study area for resistivity values lower than 100 Ωm the material is expected to have a high content of clay. Values of resistivity greater than 100 Ωm were linked to coarse grained material. These coarse materials ranged from boulders to sand; the grain size and resistivity decreased with depth. The refined model shows a better description of the different materials, making it possible to characterize the aquifer system by an unconfined, semiconfined, and confined aquifer in the apex, middle, and distal part of the fan, respectively. The study results indicate that the aquifer system bottom is composed of a layer with high clay content.

The geoelectrical methods used in this investigation demonstrated the applicability and efficiency in defining the layering and thicknesses of the different geological units in the alluvial fan. It can be concluded that the geoelectrical methods used in this research (i.e. ERT and normalized chargeability) are useful and powerful techniques for mapping the aquifer systems in the Punata alluvial fan, and in other similar areas. Further analyses for determining the mineralogy of the clay should be performed. These studies would help in the understanding how IP parameters behave in the Punata alluvial fan. Even if a refined model is proposed for the aquifer system in the Punata alluvial fan, there are some aspects that still need more investigation, such as the determination of both the thickness of the bottom layer with high clay content (Figure 7b) as well as the groundwater boundary conditions in the Punata alluvial fan. Therefore, in order to obtain additional information, it is advisable that future studies look to complement and perform more geophysical surveys, such as well-loggings, ERT and IP, and Transient Electromagnetic and Magnetic Resonance Sounding.

Author Contributions: Andres Gonzales Amaya performed the fieldwork, processed and analyzed the data. Andres Gonzales Amaya, Torleif Dahlin, Gerhard Barmen and Jan-Erik Rosberg wrote the paper.

Conflicts of Interest: The authors declare no conflict of interest.

Abbreviations

The following abbreviations are used in this manuscript:

ERT		Electrical resistivity Tomography
IP		Induced Polarization

References

1.	Blair, T.C.; McPherson, J.G. Processes and forms of alluvial fans. *Geomorphol. Desert Environ.* **2009**, 413–467.
2.	Blissenbach, E. Geology of alluvial fans in semiarid regions. *Geol. Soc. Am. Bull.* **1954**, *65*, 175–189. [CrossRef]
3.	Bridge, J.S.; Mackey, S.D. *A Revised Alluvial Stratigraphy Model, in Alluvial Sedimentation*; Blackwell Publishing Ltd.: Oxford, UK, 1993.

4. Horton, B.K.; DeCelles, P.G. Modern and ancient fluvial megafans in the foreland basin system of the central Andes, Southern Bolivia: Implications for drainage network evolution in fold-thrust belts. *Basin Res.* **2001**, *13*, 43–63. [CrossRef]

5. Bull, W.B. *Recognition of Alluvial-Fan Deposits in the Stratigraphic Record*; Society of Economic Paleontologists and Mineralogists: Tulsa, OK, USA, 1972; Volume 16, pp. 63–83.

6. Martínez, J.; Benavente, J.; García-Aróstegui, J.L.; Hidalgo, M.C.; Rey, J. Contribution of electrical resistivity tomography to the study of detrital aquifers affected by seawater intrusion–extrusion effects: The river Vélez Delta (Vélez-Málaga, Southern Spain). *Eng. Geol.* **2009**, *108*, 161–168. [CrossRef]

7. Baines, D.; Smith, D.G.; Froese, D.G.; Bauman, P.; Nimeck, G. Electrical resistivity ground imaging (ERGI): A new tool for mapping the lithology and geometry of channel-belts and valley-fills. *Sedimentology* **2002**, *49*, 441–449. [CrossRef]

8. Arjwech, R.; Everett, M.E. Application of 2d electrical resistivity tomography to engineering projects: Three case studies. *Songklanakarin J. Sci. Technol.* **2015**, *37*, 675–682.

9. Castilho, G.P.; Maia, D.F. *A Successful Mixed Land-Underwater 3D Resistivity Survey in an Extremely Challenging Environment in Amazonia*, Proceedings of the 21st EEGS Symposium on the Application of Geophysics to Engineering and Environmental Problems, Philadelphia, PA, USA, 6–10 April 2008.

10. Dahlin, T. 2d resistivity surveying for environmental and engineering applications. *First Break* **1996**, *14*, 275–283. [CrossRef]

11. Dahlin, T. The development of DC resistivity imaging techniques. *Comput. Geosci.* **2001**, *9*, 1019–1029. [CrossRef]

12. Loke, M.; Dahlin, T. A comparison of the gauss–newton and quasi-newton methods in resistivity imaging inversion. *J. Appl. Geophys.* **2002**, *49*, 149–162. [CrossRef]

13. Loke, M.; Lane, J.W., Jr. Inversion of data from electrical resistivity imaging surveys in water-covered areas. *Explor. Geophys.* **2004**, *35*, 266–271. [CrossRef]

14. Loke, M.H.; Acworth, I.; Dahlin, T. A comparison of smooth and blocky inversion methods in 2d electrical imaging surveys. *Explor. Geophys.* **2003**, *34*, 182–187. [CrossRef]

15. Crook, N.; Binley, A.; Knight, R.; Robinson, D.A.; Zarnetske, J.; Haggerty, R. Electrical resistivity imaging of the architecture of substream sediments. *Water Resour. Res.* **2008**, *44*, W00D13. [CrossRef]

16. Marshall, D.J.; Madden, T.R. Induced polarization, a study of its causes. *Geophysics* **1959**, *24*, 790–816. [CrossRef]

17. Magnusson, M.; Fernlund, J.R.; Dahlin, T. Geoelectrical imaging in the interpretation of geological conditions affecting quarry operations. *Bull. Eng. Geol. Environ.* **2010**, *69*, 465–486. [CrossRef]

18. Sumner, J.S. *Principles of Induced Polarization for Geophysical Exploration*; Elsevier: Amsterdam, The Netherlands, 2012; Volume 5.

19. Seigel, H.O. Mathematical formulation and type curves for induced polarization. *Geophysics* **1959**, *24*, 547–565. [CrossRef]

20. Slater, L.D.; Lesmes, D. IP interpretation in environmental investigations. *Geophysics* **2002**, *67*, 77–88. [CrossRef]

21. Alabi, A.A.; Ogungbe, A.S.; Adebo, B.; Lamina, O. Induced polarization interpretation for subsurface characterization: A case study of obadore, lagos state. *Arch. Phys. Res.* **2010**, *1*, 34–43.

22. Revil, A.; Binley, A.; Mejus, L.; Kessouri, P. Predicting permeability from the characteristic relaxation time and intrinsic formation factor of complex conductivity spectra. *Water Resour. Res.* **2015**, *51*, 6672–6700. [CrossRef]

23. Weller, A.; Slater, L.; Nordsiek, S. On the relationship between induced polarization and surface conductivity: Implications for petrophysical interpretation of electrical measurements. *Geophysics* **2013**, *78*, D315–D325. [CrossRef]

24. Revil, A.; Florsch, N. Determination of permeability from spectral induced polarization in granular media. *Geophys. J. Int.* **2010**, *181*, 1480–1498. [CrossRef]

25. Montenegro, E.; Rojas, F. *Potencial Hidrico Superficialy Subterraneo del Abanico de Punata*; Universidad Mayor de San Simon: Cochabamba, Bolivia, 2007.

26. United Nations Development Programme-Servicio Geológico de Bolivia (UNDP-GEOBOL). *Proyecto Integrado de Recursos Hidricos*; Cordeco: Cochabamba, Bolivia, 1978. (In Spanish)

27. Ahzegbobor, P.A. Assessment of soil salinity using electrical resistivity imaging and induced polarization methods. *Afr. J. Agric. Res.* **2014**, *9*, 3369–3378.

28. SERGEOMIN. *Mapa Geologico de Punata/Geological Map of Punata*; SERGEOMIN: La Paz, Bolivia, 2011. (In Spanish)

29. May, J.-H.; Zech, J.; Zech, R.; Preusser, F.; Argollo, J.; Kubik, P.W.; Veit, H. Reconstruction of a complex late quaternary glacial landscape in the cordillera de cochabamba (Bolivia) based on a morphostratigraphic and multiple dating approach. *Quat. Res.* **2011**, *76*, 106–118. [CrossRef]

30. BRGM-SEURECA. *Evaluacion de los Recursos de Agua y Abastecimiento en agua Potable de la Ciudad de Cochabamba, Bolivia*; Semapa: Cochabamba, Bolivia, 1990. (In Spanish)

31. Dahlin, T.; Zhou, B. A numerical comparison of 2d resistivity imaging with 10 electrode arrays. *Geophys. Prospect.* **2004**, *52*, 379–398. [CrossRef]

32. Dahlin, T.; Zhou, B. Multiple-gradient array measurements for multichannel 2d resistivity imaging. *Near Surface Geophys.* **2006**, *4*, 113–123. [CrossRef]

33. Kirsch, R. *Groundwater Geophysics*, 2nd ed.; Springer: Berlin/Heidelberg, Germany, 2009; Volume 1, p. 493.

34. American Board of Electrodiagnostic Medicine (ABEM). *Instruction Manual Terrameter LS*; ABEM: Sundbyberg, Sweden, 2016.

35. Loke, M. Res2dinv ver 3.59. 102. Geoelectrical Imaging 2D and 3D. Instruction Manual. Geotomo Software. 2010. Available online: http://www.geotomosoft.com/downloads.php (accessed on 14 November 2016).

36. Nowroozi, A.A.; Whittecar, G.R.; Daniel, J.C. Estimating the yield of crushable stone in an alluvial fan deposit by electrical resistivity methods near Stuarts Draft, Virginia. *J. Appl. Geophys.* **1997**, *38*, 25–40. [CrossRef]

37. Guérin, R.; Descloitres, M.; Coudrain, A.; Talbi, A.; Gallaire, R. Geophysical surveys for identifying saline groundwater in the semi-arid region of the central Altiplano, Bolivia. *Hydrol. Process.* **2001**, *15*, 3287–3301. [CrossRef]

38. Perez, R. Estudio geoelectrico en el valle alto de rio paria. *Geofis. Colomb.* **1995**, *1*, 27–35. (In Spanish)

39. Terrizzano, C.M.; Fazzito, S.Y.; Cortés, J.M.; Rapalini, A.E. Electrical resistivity tomography applied to the study of neotectonic structures, northwestern Precordillera Sur, Central Andes of Argentina. *J. S. Am. Earth Sci.* **2012**, *34*, 47–60. [CrossRef]

40. Giocoli, A.; Magrì, C.; Vannoli, P.; Piscitelli, S.; Rizzo, E.; Siniscalchi, A.; Burrato, P.; Basso, C.; Di Nocera, S. *Electrical Resistivity Tomography Investigations in the Ufita Valley (Southern Italy)*; Annals of Geophysics: Rome, Italy, 2008; Volume 51.

41. Odudury, P.; Mamah, L. Integration of electrical resistivity and induced polarization for subsurface imaging around Ihe Pond, Nsukka, Anambra basin, Nigeria. *Pac. J. Sci. Technol.* **2014**, *15*, 306–317.

42. Parkhomenko, E.I. *Electrification Phenomena in Rocks*; Springer Science & Business Media: Berlin/Heidelberg, Germany, 2013.

43. Koch, K.; Revil, A.; Holliger, K. Relating the permeability of quartz sands to their grain size and spectral induced polarization characteristics. *Geophys. J. Int.* **2012**, *190*, 230–242. [CrossRef]

44. Keller, G.V.; Frischknecht, F.C. *Electrical Methods in Geophysical Prospecting*; Road Research Laboratory: Osford, UK, 1966.